Biochimica et Biophysica Acta 1797 (2010) 1828–1837

Contents lists available at ScienceDirect

Biochimica et Biophysica Acta

journal homepage: www.elsevier.com/locate/bbabio

Proton transport coupled ATP synthesis by the purified yeast H^+-ATP synthase in proteoliposomes

Kathrin Förster [a], Paola Turina [b], Friedel Drepper [c], Wolfgang Haehnel [c], Susanne Fischer [a], Peter Gräber [a,*], Jan Petersen [a,1]

[a] Institut für Physikalische Chemie, Universität Freiburg, Albertstr. 23a, D-79104 Freiburg, Germany
[b] Dipartimento di Biologia, Università di Bologna, Via Irnerio 42, I-40126 Bologna, Italy
[c] Lehrstuhl für Biochemie der Pflanzen, Institut für Biologie II, Universität Freiburg Schänzlestrasse 1, 79104 Freiburg, Germany

ARTICLE INFO

Article history:
Received 16 June 2010
Received in revised form 27 July 2010
Accepted 29 July 2010
Available online 4 August 2010

Keywords:
ATP synthesis
Mitochondrial H^+-ATP synthase
K_M of phosphate
MF_0F_1
Reconstitution
Saccharomyces cerevisiae

ABSTRACT

The H^+/ATP synthase from yeast mitochondria, MF_0F_1, was purified and reconstituted into liposomes prepared from phosphatidylcholine and phosphatidic acid. Analysis by mass spectrometry revealed the presence of all subunits of the yeast enzyme with the exception of the K-subunit. The MF_0F_1 liposomes were energized by acid–base transitions (ΔpH) and a K^+/valinomycin diffusion potential (Δφ). ATP synthesis was completely abolished by the addition of uncouplers as well as by the inhibitor oligomycin. The rate of ATP synthesis was optimized as a function of various parameters and reached a maximum value (turnover number) of 120 s^{-1} at a transmembrane pH difference of 3.2 units (at $pH_{in} = 4.8$ and $pH_{out} = 8.0$) and a Δφ of 133 mV (Nernst potential). Functional studies showed that the monomeric MF_0F_1 was fully active in ATP synthesis. The turnover increased in a sigmoidal way with increasing internal and decreasing external proton concentration. The dependence of the turnover on the phosphate concentration and the dependence of K_M on pH_{out} indicated that the substrate for ATP synthesis is the monoanionic phosphate species $H_2PO_4^-$.
© 2010 Elsevier B.V. All rights reserved.

1. Introduction

Membrane-bound H^+-ATP synthases (H^+-translocating adenosine triphosphatase EC 3.6.1.14) synthesize ATP from ADP and inorganic phosphate using the energy of a transmembrane electrochemical potential difference of protons [1–3]. They occur in the plasma membranes of bacteria, in the thylakoid membrane of chloroplasts and in the inner membrane of mitochondria [4–8]. H^+-ATP synthases consist of a hydrophilic F_1-part (subunits $\alpha_3\beta_3\gamma\delta\varepsilon$) containing the nucleotide and P_i binding sites and of a hydrophobic membrane integrated F_0-part containing the proton binding sites (subunits ab_2c_{10-12}) (subunit composition and nomenclature of *E. coli*). The kinetics of the enzyme is described by the binding change theory which explains the cooperativity of the three catalytic sites by rotation of the γ-subunit within the $\alpha_3\beta_3$-barrel [9,10]. The first high resolution structure of the F_1-part, from bovine heart mitochondria, corroborated this theory [11]. A crystal structure of the holo-enzyme (F_0F_1) was obtained for the yeast mitochondrial enzyme [12], which revealed a ring structure with 10 c-subunits and their interaction with the γ-subunit. Anti-clockwise (viewed from the membrane side) rotation of the γ-subunit during ATP hydrolysis was observed in bacterial F_1-parts [13]. Movements of the γ- and ε-subunit relative to the stator subunits during ATP synthesis and opposite movements during ATP hydrolysis have been shown by single pair fluorescence spectroscopy with membrane integrated EF_0F_1 [14,15].

To investigate the mechanism of coupling between proton transport and ATP synthesis H^+-ATP synthases from bacteria and chloroplasts have been isolated, purified and reconstituted into liposomes. In these reconstituted systems high rates of ATP synthesis (up to 200 s^{-1}) in response to ΔpH and Δφ generated in acid–base transitions have been reported — see e.g. [16–21]. A tremendous amount of biochemical, structural and functional work has been carried out with the F_1-part of mitochondrial H^+-ATP synthases (MF_0F_1). However, much less is known about the coupling between proton transport and ATP synthesis. ATP synthesis by bovine sub-mitochondrial particles (SMP) driven by acid–base transition was reported [22], and from that work a turnover number in the order of 50 s^{-1} can be calculated under the assumption that the H^+-ATP synthase represents 10% of the total protein. Several isolation procedures of mitochondrial MF_0F_1 have been reported and after reconstitution into liposomes functional studies reveal that the

Abbreviations: F_0, transmembrane sector of the H^+-ATP synthase; F_1, hydrophilic, extrinsic sector of the H^+-ATP synthase; ΔpH, transmembrane difference of pH; Δφ, bulk-to-bulk transmembrane electrical potential difference; $\Delta\tilde{\mu}_{H^+}$, transmembrane difference of electrochemical potential of protons; SMP, submitochondrial particles; PMSF, phenylmethylsulfonyl fluoride; HEPES, (4-(2-hydroxyethyl)-1-piperazineethanesulfonic acid); DDM, dodecylmaltoside; BN-PAGE, Blue Native Polyacrylamide Gel Electrophoresis; SDS-PAGE, Sodium Dodecyl Sulfate Polyacrylamide Gel Electrophoresis; Tricine, N-[2-Hydroxy-1,1-bis(hydroxymethyl)ethyl] glycine

* Corresponding author. Tel.: +49 761 2036192; fax: +49 761 2036189.
E-mail address: peter.graeber@physchem.uni-freiburg.de (P. Gräber).
[1] Present address: Department of Biochemistry & Molecular Biology, Monash University, Clayton, Vic 3800, Australia.

0005-2728/$ – see front matter © 2010 Elsevier B.V. All rights reserved.
doi:10.1016/j.bbabio.2010.07.013

enzyme appeared to be able to hydrolyze ATP, to energize the membrane by proton transport, and to catalyze ATP-P_i exchange — see e.g. [23–26]. Detectable ATP synthesis rates were reported, when MF_0F_1 was co-reconstituted with bacteriorhodopsin with turnover numbers ranging between 10^{-4} and 10^{-3} s^{-1} [23,27,28]. These results contrast with the maximal turnover number of 440 s^{-1} previously estimated in submitochondrial particles [29]. The reason for the low rates could well have been the low levels of protonmotive force achievable with reconstituted bacteriorhodopsin [30]. High proton motive forces can be established by acid–base transitions. However, such studies with reconstituted MF_0F_1 have not been reported yet.

To obtain high ATP synthesis activities several problems must be solved: 1) The mitochondrial H^+-ATP synthase is more complex than the corresponding bacterial and chloroplast enzymes. It has 20 different subunits and it is possible that an important subunit is lost either during isolation or during the reconstitution procedure. 2) MF_0F_1 is able to form supramolecular complexes [31–33] and electron microscopy studies, both of detergent-solubilised MF_0F_1 complexes and of mitochondrial membranes revealed an angled arrangement of the monomers in dimers, and a ribbon-like organization in higher order oligomers [34–36]. MF_0F_1 oligomerization imposes a curvature on the inner mitochondrial membrane, and the resulting invaginations have been proposed to act as proton traps improving the efficiency of ATP synthesis [36,37]. However, the functional significance of MF_0F_1 oligomerization is not yet fully understood, in particular it is not known whether the monomeric form is capable of high activities. 3) The purified MF_0F_1 detergent micelle must be reconstituted into liposomes in a functionally active form. 4) The optimal conditions for measuring high activities must be established.

In this work MF_0F_1 was isolated, the subunit composition was determined by mass spectrometry and the monomeric enzyme was reconstituted into liposomes. Acid–base driven ATP synthesis by such monomeric enzyme resulted in rates as high as 120 s^{-1} .Moreover, it is shown that the substrate for ATP synthesis is the monoanionic species $H_2PO_4^-$.

2. Materials and methods

2.1. Cell growth and MF_0F_1 purification

Saccharomyces cerevisiae cells of the strain YRD15 (MATα his3-11,3-15 leu2-3,2-112, ura3-251,3-373[rho$^+$]) [38] were grown in well-aerated SACC$^+$ media [1% (w/v) yeast extract, 0.12% (w/v) $(NH_4)_2SO_4$, 0.1% (w/v) KH_2PO_4, 0.01% (w/v) $CaCl_2$, 0.0005% (w/v) $FeCl_3$, 0.07% (w/v) $MgCl_2$, 0.05% (w/v) NaCl, 2% (v/v) ethanol] supplemented with 20 mg/l of each leucine, histidine and uracil and stored at −80 °C. A total of 100 g cells was thawed in 200 ml of buffer A1 (10 mM Tris/HCl pH 7.0, 250 mM sucrose, 5 mM 6-aminohexanoic acid) and phenylmethylsulfonyl fluoride was added to a final concentration of 0.0025% (w/v). MF_0F_1 was isolated similarly as described in [12]. Cells were disrupted with glass beads at 4 °C as previously described [24] and the cell debris was removed by centrifugation at 1000 *g* for 30 min in a Beckman JA-16.250 rotor at 4 °C. Crude mitochondria were isolated by centrifugation of the supernatant at 23000 *g* for 30 min in the same rotor at 4 °C. The pellet was resuspended in 40 ml buffer B1 (20 mM HEPES, 250 mM sucrose, 5 mM 6-aminohexanoic acid, 40 mM NaCl, 4 mM $MgCl_2$ and 1 mM EDTA, titrated to a pH of 7.65 with NaOH). Submitochondrial particles (SMP) were prepared by sonicating the mitochondria for 3 min in a Branson Sonifier 250 (Output level 2, Duty Cycle 40%). Large particles were removed by centrifugation for 20 min at 4000 *g* in a Beckman JA-20 rotor at 4 °C. The SMP were collected by centrifugation for 30 min at 100000 *g* in a Beckman 60Ti rotor at 4 °C. The pellet was homogenized in 75 ml buffer B1 containing 0.0025% phenylmethylsulfonyl fluoride and 1.4% dodecylmaltoside and stirred for 40 min at room temperature. After addition of 75 ml cold B1, insoluble material was removed by centrifugation (30 min, 180000 *g* in a Beckman 60Ti rotor). The supernatant was applied to a 16 ml HQ20 column equilibrated with buffer C1 (20 mM HEPES, 250 mM sucrose, 1 mM EDTA, 4 mM $MgCl_2$, 5 mM 6-aminohexanoic acid, 1 mM dithiothreitol, 100 mM NaCl, 0.05% DDM, titrated to a pH of 7.65 with NaOH). The protein was eluted in a step gradient by increasing the NaCl concentration in buffer C1 from 100 mM NaCl to 184 mM NaCl. Fractions containing protein (determined photometrically) were pooled (approx. 20 ml) and concentrated in an Amicon Ultra-15 centrifugal filter (molecular weight limit 10 kDa). Gel filtration of the concentrated enzyme was carried out in buffer C1 with a 16/90 Sephacryl 300 column. Fractions containing MF_0F_1 were pooled (20 ml), concentrated as described above to a protein concentration of 5–10 μM, rapidly frozen and stored in liquid nitrogen. Total yield was approximately 10 mg. The concentration of MF_0F_1 was measured spectroscopically using the absorption coefficient at 280 nm calculated according to [39]. The absorption coefficients of the subunits are shown in Supplementary Table S1. The subunit composition of our MF_0F_1 preparation was determined by HPLC-electrospray mass spectrometry and, using the subunit stoichiometry reported in [40] ($\alpha_3\beta_3\gamma5\delta$ 4ad89$_{10}$HfJe, see Supplementary Table S1 for nomenclature). In the following we used the absorption coefficient $\varepsilon_{280} = 279\,130\ M^{-1}\ cm^{-1}$ for all concentration measurements. We assumed that all MF_0F_1 added to the reconstitution mixture was correctly incorporated into the membrane, which implies that the enzyme activities given in this work are the minimal activities.

2.2. Detection of monomeric and dimeric MF_0F_1 by Blue Native PAGE

SDS-polyacrylamide gel electrophoresis (SDS-PAGE) was carried out as described in [41]. The protein sample was incubated in 20 mM Tris pH 8, 2% (w/v) SDS, 1 mM DTT, 10% (v/v) glycerol and 0.04% bromophenol blue for 10 min at 95 °C and applied to a discontinuous acrylamide gel (13% gel overlaid with 4% sample gel).

Monomeric and dimeric MF_0F_1 were separated with Blue Native Polyacrylamide Gel Electrophoresis (BN-PAGE) as described previously [31]. MF_0F_1 was solubilized with Triton X-100 to protein ratios between 0.6 and 1.2 g/g protein from the isolated mitochondrial membranes. The solubilised proteins were applied to an acrylamide gradient gel (linear 4–13% gradient, overlaid with a 4% sample gel).

2.3. Protein identification by HPLC–electrospray mass spectrometry

Lanes of a SDS-PAGE (13%) were cut into 38 horizontal 1 mm slices. Each slice was processed individually for establishing abundance profiles of identified peptides. Proteins were modified by iodoacetamide and in-gel digested as described [42]. Peptide mixtures were separated for nano-LC–ESI-MS/MS using a FAMOS Autosampler (Dionex), an Ultimate inert HPLC (Dionex) and an Agilent HPLC 1100 pump connected to the nano-ESI-Source of a Finnigan LTQ-FT (Thermo Electron) for online mass detection. Peptides were first collected on a trap column (0.1 × 15 mm, Zorbax Eclipse XDB-C18, 5 μm, Agilent Technology) for desalting and concentrating followed by separation on an analytical column made up by a fused silica emitter (0.075 × 150 mm, 6 μm, Proxeon Biosystems) filled with Pro C18, 3 μm (YMC). Peptides were eluted using a linear gradient from 97% water, 3% acetonitrile and 0.1% formic acid to 80% acetonitrile, 20% water and 0.1% formic acid within 60 min at a flow rate of 0.15 μl min^{-1}. Mass spectrometric detection consisted of full scans at a resolution of 25000 followed by data dependent selected ion scans at a resolution of 50000 and low resolution MS/MS scans using a dynamic exclusion of parent ion masses for 60 s.

The MS and MS/MS spectra were searched against *Saccharomyces cerevisiae* protein sequences deposited at the Uniprot database (release Feb 10, 2009) using an in-house installation of the program OMSSA (version 2.1) [43] as described [44]. Peptide hits were considered

significant if the precursor and product ion masses matched within 2 ppm and 0.5 rel. mass units, respectively, and if the E-value was below 0.01. Only the best hit per spectrum was considered. These criteria resulted in a peptide false positive rate of 0.1%. The peptide score was computed from the P-value of the program OMSSA as $-\log_{10}(P)$. Protein intensities were calculated as the sum of peptide integrated ion currents using the MSQuant program version 1.5 [45] and were used to compute protein distribution profiles [46]. For low intensity peptides which were not selected for data dependent MS/MS scans ion currents were manually integrated at a given mass over charge ratio using the Xcalibur Software (Thermo Electron). The latter method was used for subunit g.

2.4. Reconstitution of MF_0F_1 into liposomes

The reconstitution of MF_0F_1 into liposomes was carried out similarly as described in [47]. Preformed liposomes from phosphatidylcholine and phosphatidic acid (mass ratio 19:1) were prepared by sonication (3×30 s in a Branson Sonifier 250, Output level 4, Duty Cycle 90%) and by dialysis against buffer D1 (10 mM Tricine, 0.2 mM EDTA, 2.5 mM $MgCl_2$ and 0.25 mM dithiothreitol, titrated to pH 8.0 with NaOH). The lipid concentration after dialysis was 16 g/l. The liposomes were rapidly frozen and stored in liquid nitrogen. The size distribution of the liposomes was determined by photon correlation spectroscopy using a Zetamaster S/90° ZEN 5002, Malver Instruments. For reconstitution of MF_0F_1, 150 µl liposomes were thawed and MF_0F_1 (6 µl, 7.5 µM in buffer C1), $MgCl_2$ (final concentration 2.5 mM), Triton X-100 (24 µl, final concentration 0.8% (w/v)) and 119 µl buffer E1 (20 mM succinate, 20 mM Tricine, 60 mM NaCl, 0.6 mM KCl, titrated to pH 8.0 with NaOH) were added. The reconstitution mixture was stirred slowly at room temperature for 1 h. Addition of Biobeads (35 mg per 100 µl of the protein/lipid/detergent solution) led to the removal of Triton X-100 and the insertion of MF_0F_1 into the liposome membrane [48]. In the end, the lipid concentration of the proteoliposomes was approximately 8 g/l with a MF_0F_1 concentration of 150 nM.

2.5. Measurement of ATP synthesis

The rate of ATP synthesis was measured at 25 °C similar as described earlier [17]. The proteoliposomes were energized by an acid–base transition and an additional K^+/valinomycin diffusion potential. The ATP concentration was monitored continuously with luciferin/luciferase (Roche) in a luminometer (LKB 1250). In order to generate the ΔpH, the proteoliposomes were incubated in the acidic medium (F1: 20 mM succinate, 0.6 mM KOH, 4 mM $MgCl_2$, 0.1–15 mM NaH_2PO_4, 0.4 mM ADP, 20 µM valinomycin (freshly added)). To generate different ΔpH during the acid–base transition the acidic medium was titrated with NaOH to pH values between 4.7 and 6.7. The pH of the basic medium was constant: 250 mM Tricine, 120 mM KOH, 0.1–15 mM NaH_2PO_4, 4 mM $MgCl_2$, 0.4 mM ADP, titrated to pH 8.0 with NaOH.

ATP synthesis and detection of ATP with the luciferin/luciferase assay were carried out simultaneously as follows: 880 µl of the basic medium were mixed with 20 µl luciferin/luciferase reagent, placed in the luminometer and the base line was recorded. Proteoliposomes (15 µl, MF_0F_1 concentration 150 nM) were mixed with 100 µl acidic medium. The incubation time was varied between 2 min at $pH_{in}=4.8$ and 30 min at $pH_{in}=6.8$ at 25 °C. ATP synthesis was initiated by injection of 100 µl of this solution with a Hamilton syringe directly into the basic medium. Supplementary Table S2, supplement shows the resulting concentrations inside and outside the proteoliposomes after the acid–base transition during ATP synthesis. The increase of the ATP concentration was followed by the luminescence intensity. When the signal reached a constant level, it was calibrated by addition of an ATP standard solution. The internal pH was assumed to be equal to the pH measured after equilibration of 100 µl of the acidic medium with 15 µl of the proteoliposomes. The pH of the strongly buffered basic medium did not change after addition of the acidified liposomes, i.e. the pH_{out} value was always 8.0. In addition to the transmembrane pH-difference a K^+/valinomycin diffusion potential was generated. The internal K^+ concentration was 0.6 mM, the external K^+ concentration was 106 mM. The transmembrane electric potential difference was estimated from the Nernst equation as 133 mV.

The luminescence time traces were fitted by a combination of an exponential and a linear function using the software package Origin. The initial rates were calculated from the fitted function. All given values are the arithmetic mean of triplicate measurements with the standard deviation.

3. Results

3.1. Subunit composition and oligomeric state of the isolated MF_0F_1

MF_0F_1 was isolated from yeast cells and purified as described in Materials and methods. Fig. 1A shows the results of the SDS-PAGE after the final purification step. The subunits were identified by mass spectrometric analysis and named according to the nomenclature of the Uniprot database. A comparison with earlier nomenclature is given in Supplementary Table S1. The oligomeric state of the isolated MF_0F_1 was analysed using blue native gel electrophoresis. Purified MF_0F_1 and for comparison MF_0F_1 solubilised from mitochondrial membranes with increasing ratios of Triton X-100 to protein were separated by BN-PAGE (Fig. 1B). At low Triton X-100 concentrations (lanes II and III) two dominant complexes were found, which were previously identified as monomeric and dimeric MF_0F_1 with the approximate molecular masses of 500 and 1000 kDa respectively [31,49]. At the highest Triton X-100 concentration (lane IV) the band attributed to the dimeric MF_0F_1 had disappeared, as reported previously [31]. Densitometric analysis of the gel revealed approx. 60% of the dimeric form in lane II. The DDM solubilised, purified enzyme (lane I) showed less than 1% of the dimeric form. We conclude that our purified MF_0F_1 only contains the monomeric form.

3.2. Subunit composition by HPLC–electrospray mass spectrometry

The SDS-PAGE gel of MF_0F_1 was analysed by HPLC–electrospray mass spectrometry as described in Materials and methods. Fig. 2A shows the analysed lane and its optical density profile. The distribution profiles for the MF_0F_1 subunits are given in Fig. 2 B–D, and show that the preparation contained all subunits except subunit K. Most of the subunits have been identified with sequence coverage above 60% as summarised in Table 1. Subunits 8, a, g and 9 have been detected with a lower sequence coverage which could be due to the hydrophobic nature of protein subunits 8, a and 9 and the lysine-rich sequence of subunit g. Subunit 9 was found in our SDS-PAGE at a molecular weight of 84 kDa (see Table 1 and Fig. 1), indicating that it was present as an oligomer as described earlier [31,50]. Surprisingly, and at variance with what has been found in previous preparations of yeast MF_0F_1 [12,51], the dimer-specific e- and g-subunits were also detected. Subunit g was identified with one peptide at the apparent molecular weight of 21.7 kDa (Table 1 and Fig. 2B, grey solid line). This is about twice as much as the calculated molecular weight of the mature protein, and also twice the apparent molecular weight reported previously [31,52]. Inspection of the HPLC–MS ion chromatograms showed that the mass of the identified peptide ion was also present at approximately 11 kDa, however at a lower intensity (Fig. 2, grey dashed line). Therefore, it appears that subunit g is present both as a dimer, as found in rat MF_0F_1 [53], and as a monomer.

Due to its high sensitivity, the mass spectrometric analysis allowed to detect also subunits of MF_0F_1 which were not visible in the Coomassie stained SDS-gel, either due to poor staining, or to co-migration in a single band (see e.g. subunit ε, J and 8 in Fig. 2). In addition to the MF_0F_1

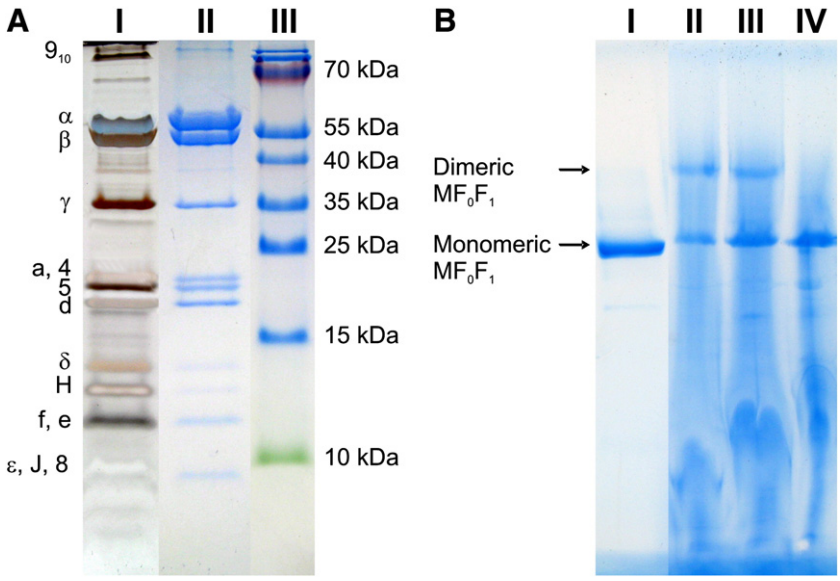

Fig. 1. Subunit composition and oligomerization of MF_0F_1. (A) SDS-PAGE (13%) of purified MF_0F_1 from *S. cerevisiae*. I: Silver stained. II: Stained with Coomassie Brilliant Blue. III: Molecular weight standard. (B) Blue Native PAGE (linear 4–13% gradient gel, overlaid with a 4% sample gel) of purified MF_0F_1 from *S. cerevisiae* (I) and of mitochondria solubilised at varying Triton X-100 to protein ratios respectively (II: 0.6 g/g, III: 0.8 g/g, IV: 1.2 g/g). The positions of the monomeric and dimeric forms of MF_0F_1 are indicated.

subunits, we also identified a number of peptides from other mitochondrial proteins, which were neither visible in the Coomassie nor in the silver stained SDS-gel (Fig. 1).

3.3. ATP synthesis by acid–base transitions

After reconstitution of MF_0F_1 in phosphatidylcholine/phosphatidic acid liposomes, acid–base transitions were carried out and ATP synthesis was measured as described in Materials and methods. Fig. 3 shows some original traces from these experiments. Fig. 3A was obtained at an internal pH of 5.0 and an external pH of 8.0 ($\Delta\varphi = 133$ mV). The baseline resulted from the ATP content of the commercial ADP present in the basic medium. The acidified proteoliposomes were injected at time $t = 0$ (indicated by the arrow). The injection resulted in a small mixing artefact, followed by an increase in luminescence due to ATP synthesis. The rate of luminescence increase was highest at $t = 0$, decreasing to zero after approximately 15 s. This decrease of the rate is due to the decay of the transmembrane protonmotive force after the acid–base transition. The initial rate, i.e. the slope at $t = 0$, was $v = 175\ nM\ s^{-1}$ (see Fig. 3A). By taking into account the MF_0F_1 concentration in the reaction assay (2.0 nM), this gives a turnover value of $v/E_0 = 88\ s^{-1}$. The total amount of ATP generated in the acid–base transition (ATP yield) is also shown ($\Delta ATP_{total} = 175$ ATP per MF_0F_1). When the transmembrane $\Delta\tilde{\mu}_{H^+}$ was abolished by addition of 50 mM NH_4Cl to the basic medium, no ATP synthesis could be detected (Fig. 3B). When 10 μg/ml oligomycin, which blocks proton flow by binding to MF_0F_1, was added to the acidic and the basic medium, again no ATP synthesis could be observed (Fig. 3C).

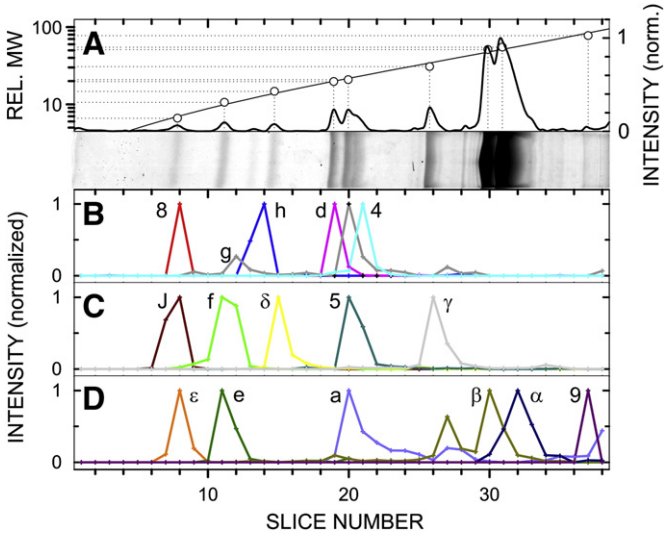

Fig. 2. Mass spectrometric determination of subunit composition of MF_0F_1. SDS-Page (13%) of purified MF_0F_1 from *S. cerevisiae* after staining with Coomassie Brilliant Blue. (A) Optical density profile of the gel lane after background correction (bold, right axis); the relative molecular weight (Rel. MW) of the subunits marked with open circles are used for interpolation (dashed lines, left axis). (B)–(D): Distribution profiles for subunits of MF_0F_1. The normalized intensity calculated as the sum of integrated peptide ion currents for all peptides identified for one subunit by HPLC–MS/MS is plotted against the position of the individual gel slice. For the sake of clarity the data are presented in three plots.

3.4. Catalytically active MF_0F_1 — monomer or dimer?

As shown in Fig. 1B, the purified MF_0F_1 was obtained in its monomeric form. During reconstitution of MF_0F_1 into preformed liposomes, detergent is added to destabilize the bilayer membrane and the hydrophobic parts of the MF_0F_1 micelles interact with the liposome membrane. Removal of the detergent by BioBeads leads to an integration of the enzyme into the membrane with the hydrophilic F_1-part directed to the outside [48,54]. If more than one MF_0F_1 is inserted into the membrane of a single liposome, the formation of dimers is possible, even if only monomers were present at the beginning of the reconstitution procedure. The average number of MF_0F_1 per liposome can be estimated as follows. As determined by photon correlation spectroscopy [55], the average diameter of the proteoliposomes is 150 nm. Assuming that the thickness of the membrane is 8 nm (sum of the inner (r_i) and outer (r_o) surface, $O = 4\pi\ (r_i^2 + r_o^2) = 4\pi\ (67^2 + 75^2)\ nm^2 = 1.3\ 10^5\ nm^2$), a surface area of $1.3\ 10^5\ nm^2$ is obtained. The average area of a lipid molecule is $0.6\ nm^2$ [56], i.e. an average liposome contains $2.2\ 10^5$ lipid molecules. The lipid concentration during reconstitution was 8 mg/ml or 10.5 mM (calculated with an average molecular mass of the lipids of 760 g/mol) which corresponds to a liposome concentration of 48 nM.

Table 1
Mass spectrometric identification of subunits of yeast MF_0F_1 following in-gel digestion by trypsin of the slices cut from Coomassie stained lane of SDS-PAGE (Fig. 2).

Subunit	Protein ID[a]	Slice	Gel MW[b] (kDa)	MW[c] (kDa)	Number of amino acids	Coverage[d] %	Max. intensity[e]	Number of peptides[f]
8	P00856	8	7.1	5.8	48	22.9	4.2E+04	2
epsilon	P21306	8	7.1	6.6	61	93.4	6.3E+07	32
J	P81450	8	7.1	6.7	59	94.9	8.6E+06	19
f	Q06405	11	9.7	10.6	95	62.1	1.5E+07	21
e	P81449	11	9.7	10.7	95	72.6	8.0E+06	19
H	Q12349	14	13	10.4	92	100	5.9E+06	39
delta	Q12165	15	14.2	14.6	138	91.3	3.4E+07	54
d	P30902	19	20	19.7	173	91.3	2.8E+08	68
5	P09457	20	21.7	20.9	195	93.3	1.8E+08	59
a	P00854	20	21.7	27.9	249	17.7	3.8E+06	9
g	Q12233	20	21.7	12.9	115	9.6	3.9E+04	1
4	Q6B1V4[g]	21	23.6	23.2	209	80.9	2.4E+08	64
gamma	P38077	26	35	30.6	278	87.8	2.1E+08	61
beta	P00830	30	47.8	51.1	478	89.5	1.7E+08	66
alpha	P07251	33	60.6	54.9	510	84.1	2.1E+08	71
9	P61829	37	83.8	7.8	76	40.8	3.7E+04	1

[a] Identifier from Uniprot database.
[b] Molecular weight for gel slice as determined by extrapolation.
[c] Calculated molecular weight of mature protein.
[d] Sequence coverage of total sequence by peptides detected.
[e] Maximum intensity (sum of peptide integrated ion currents).
[f] Number of non-redundant peptides detected.
[g] Q6B1V4 differs from swissprot id P05626 at positions Leu11 (Ala in P05626), which is within the transit sequence, and Ala171 (Arg in P05626) which has been identified (data not shown).

The MF_0F_1 concentration during reconstitution was 150 nM. Assuming that all enzymes are reconstituted into the membrane, each liposome would contain on average 3 MF_0F_1. Based on these considerations, a dimerisation of MF_0F_1 in the membrane was possible under our conditions and, therefore, the rate shown in Fig. 3 might be due to both monomeric and dimeric enzymes.

To resolve this ambiguity, the MF_0F_1 concentration during reconstitution was varied from 0.1 to 10 MF_0F_1 per liposome, and the initial rate of ATP synthesis per MF_0F_1 was measured. While a significant dimerisation is unlikely in the range between 0.1 and 1 MF_0F_1 per liposome, it could occur in principle in the case of more than 1 MF_0F_1 are reconstituted per liposome. However, as shown in Fig. 4A, the turnover (rate per enzyme) did not depend on the number of MF_0F_1 per liposome in the whole range between 0.1 and 10 MF_0F_1 per liposome. In addition to the rate, the total amount of ATP per MF_0F_1 (ATP yield) generated in the acid–base transition (ΔATP_{total}, see Fig. 3) was measured. It was constant in the range between 0.1 and 1 MF_0F_1 per liposome and decreased at higher ratios (Fig. 4B). Whereas the initial rate (turnover) depends only on pH_{out}, pH_{in}, $\Delta\varphi$ and the substrate concentrations the ATP yield depends, additionally, on the

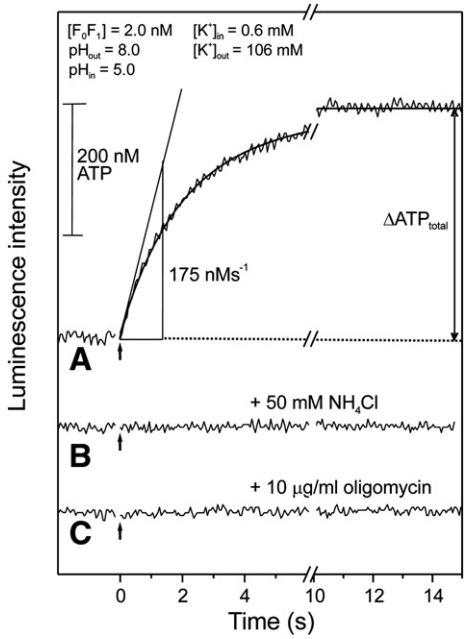

Fig. 3. ATP synthesis catalyzed by MF_0F_1 liposomes. The ATP concentration was measured with luciferin/luciferase as a function of time after the acid–base transition. The acidified proteoliposomes were injected into the basic medium resulting in a small mixing artefact (gap). The arrows indicate the starting point of the reaction t = 0. The slope directly after mixing (t = 0) is the initial rate of ATP synthesis, calculated from the fitted curve (solid line). ΔATP_{total} is the amount of ATP synthesized in the acid–base transition after 15 s (ATP yield). (A) ATP synthesis after an acid–base transition at $pH_{in} = 5.0$, $pH_{out} = 8.0$ and $\Delta\varphi \approx 133$ mV. (B) same conditions as in A but with addition of 50 mM NH_4Cl in the basic medium. (C) Same conditions as in A but in the presence of 10 µg/ml oligomycin in the acidic and the basic medium.

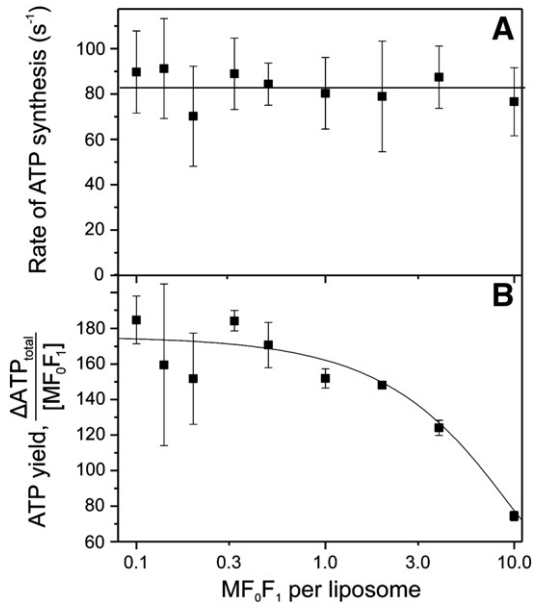

Fig. 4. ATP synthesis activity as a function of the number of MF_0F_1 per liposome. Experimental conditions as described in Fig. 3. The number of MF_0F_1 per liposome was varied by changing the MF_0F_1 concentration during reconstitution in a range between 5 and 480 nM at constant concentration of liposomes (48 nM). Each point is the average of three experiments with standard deviation. (A)Initial rate of ATP synthesis per MF_0F_1 (turnover). (B) Total amount of synthesized ATP per MF_0F_1 (ATP yield) measured 15 s after the acid–base transition (see Fig. 3).

internal buffer capacity of the liposomes, i.e. on the amount of protons stored inside. After the acid–base transition, the protons stored in the inner aqueous phase flow back to the external phase via a basal proton flux (through the membrane) and a phosphorylation coupled proton flux (through MF_0F_1). If more than one MF_0F_1 is present in the membrane, the phosphorylation coupled proton flux is distributed between two or more enzymes, which decreases the number of protons available for each enzyme, and, accordingly, the ATP yield (amount of ATP synthesized per MF_0F_1). Therefore, the observed reduction of the yield indicates that, at stoichiometric ratios higher than 1 MF_0F_1 per liposome in the reconstitution medium, more than one enzyme was reconstituted per liposome.

Comparing the ATP synthesis rate and the ATP yield as a function of MF_0F_1 concentration, we conclude that monomeric MF_0F_1 catalyzes high rates of proton transport driven ATP synthesis and that dimerisation, if it occurs, does not influence the ATP synthesis.

3.5. Optimization of reaction conditions for ATP synthesis

To obtain high rates of ATP synthesis, the reaction conditions of the acid–base transition have been optimized with respect to pH_{in} and pH_{out}. The electric potential difference $\Delta\varphi = 133$ mV as well as the substrate concentrations were kept constant ($[P_i] = 5$ mM, [ADP] = 0.4 mM). The incubation time of the proteoliposomes in the acidic medium was varied and the time chosen for further measurements was the time at which the rate showed no further increase with increasing incubation time. The incubation times were 30 min for $6.5 < pH_{in} < 6.8$, 10 min for $6.2 < pH_{in} < 6.4$, and 2 min for $4.8 < pH_{in} < 6.0$. The longer incubation time needed at the highest pH_{in} was expected due to the lower concentration of the most permeant neutral and monoanionic forms of succinate. The dependence of the rate of ATP synthesis on pH_{in} at $pH_{out} = 8.0$ is shown in Fig. 5A. The rate shows a sigmoidal dependence on pH_{in} reaching a maximal rate of 80 s^{-1} at $pH_{in} = 5.0$. Incubation in the acidic medium might lead to an inactivation of the enzyme, especially at the highest proton concentrations. A small inactivation was observed only at the highest proton concentration ($pH_{in} = 4.8$). This rate is shown by the open square in Fig. 5A. The inactivation has been corrected by comparing the rates at $pH_{in} = 5.2$ with and without preincubation at $pH_{in} = 4.8$, as described in Fig. S1 [57]. This correction increased the rate slightly (full square at $pH_{in} = 4.8$). The observation of a maximal rate indicates that the enzyme has reached a fully protonated state, so that an increase of the proton concentration did not lead to a further increase of the rate.

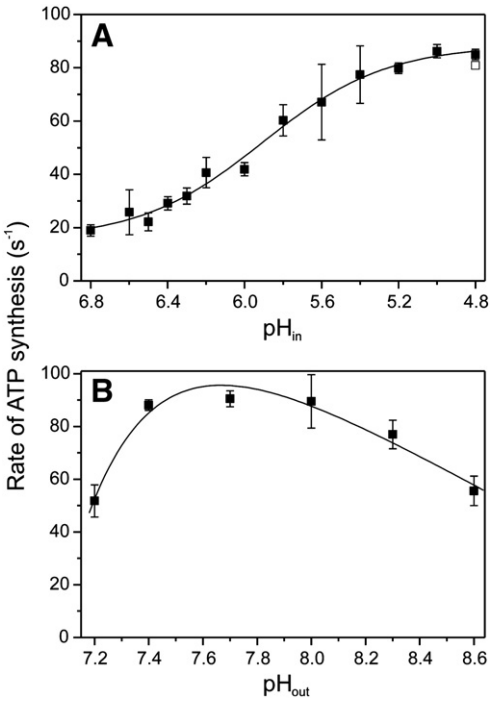

Fig. 5. (A) Rate of ATP synthesis as a function of pH_{in} at constant $pH_{out} = 8.0$. Other conditions as described in Fig. 3. pH_{in} is varied between 4.8 and 6.8. The open symbol indicates the directly measured rate at the highest proton concentration. The closed symbol is the rate corrected as described in Fig. S1. (B) Rate of ATP synthesis as a function of pH_{out} at constant $pH_{in} = 5.2$. Each point is the average of three experiments with standard deviation. pH_{out} is varied between 7.2 and 8.6.

The dependence of the rate of ATP synthesis on pH_{out} at constant $pH_{in} = 5.2$ is shown in Fig. 5B. With increasing pH_{out}, the rate reached a maximum at $pH_{out} = 7.7$ followed by a decrease. The increase in the rate with decreasing proton concentration outside indicates that at $pH_{out} = 7.2$, the proton release from the enzyme to the outside is rate limiting and that this step is facilitated at low outside proton concentrations. However, the decrease of the rate at $pH_{out} > 8.0$ was unexpected and cannot be explained by deprotonation of the enzyme. One possibility for this effect might be a limited supply of a substrate. In the measurements shown in Fig. 5A and B, the total phosphate concentration was kept constant, however, the relative concentration of the different phosphate species depended on the pH_{out} and the observed decrease in the rate might be due to a limiting concentration of the phosphate species binding to the enzyme. This consideration prompted us to investigate the phosphate dependence of the rate in detail.

3.6. The phosphate species involved in ATP synthesis

The pH_{out} determines the protonation state of substrates and products. It is still an open question which protonation state of phosphate binds to MF_0F_1 during ATP synthesis. Therefore, the rate of ATP synthesis was measured as a function of the phosphate concentration at different pH_{out}. In Fig. 6A the relative rates of ATP synthesis are shown as a function of the total P_i concentration at different pH_{out} between 7.2 and 8.6. At each pH_{out} the rate could be described by Michaelis–Menten kinetics:

$$\frac{v}{v_{max}} = \frac{[P_i(\text{total})]}{K_M + [P_i(\text{total})]}, \quad K_M = \frac{k_{cat} + k_{-1}}{k_1} \tag{1}$$

where K_M is the Michaelis–Menten constant referring to the total P_i concentration and $v_{max} = k_{cat}[E_0]$ is the maximal rate. The solid lines in Fig. 6A were calculated from Eq. (1), and the parameters v_{max} and K_M were obtained from nonlinear regression analysis. The K_M values increased from 0.4 mM at $pH_{out} = 7.2$ to 6 mM at pH_{out} 8.6 (see Fig. 6B). The maximal rates increased with pH_{out} from 60 s^{-1} at pH_{out} 7.0 to 120 s^{-1} at $pH_{out} = 8.6$ (see Fig. 7A). If the enzyme accepts only one protonation state of phosphate as substrate in ATP synthesis, the relevant parameter in kinetics is the concentration of this species, and not the total phosphate concentration. Therefore, the data was analysed as follows: P_i forms three ionic species in aqueous solution and the fraction of each species can be calculated from the dissociation constants of the three protonation states (K_1, K_2, K_3). The dissociation constants are corrected for the ionic strength of the reaction medium (I = 0.14 M) as described in [58] resulting in $pK_1 = 1.83$, $pK_2 = 6.89$ and $pK_3 = 12.07$. For details see Supplementary Table S3.

Using these pK-values, the fraction of the monoanionic species $H_2PO_4^-$ is calculated from Eq. (2) and shown as function of pH_{out} in Fig. 6B.

$$\alpha = \frac{[H_2PO_4^-]}{[P_i(\text{total})]} = \frac{K_1[H^+]^2}{[H^+]^3 + K_1[H^+]^2 + K_1K_2[H^+] + K_1K_2K_3} \tag{2}$$

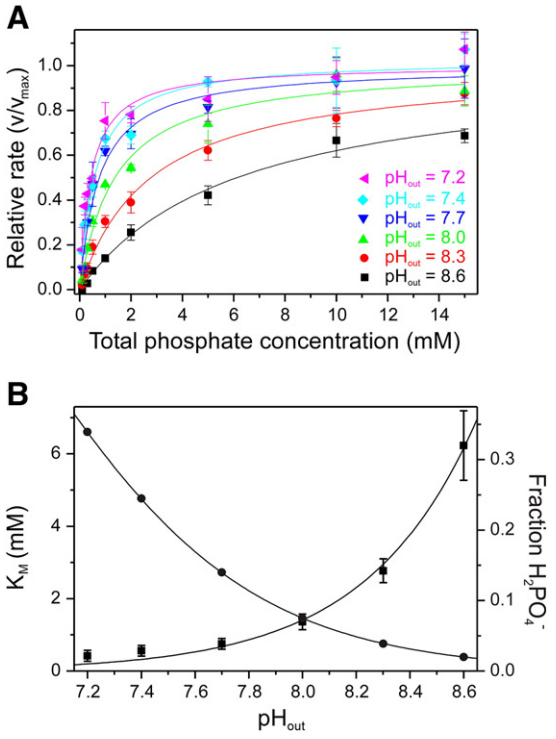

Fig. 6. Rate of ATP synthesis as a function of phosphate concentration. (A) Relative rates of ATP synthesis as a function of the total phosphate concentration at different pH between $pH_{out} = 8.6$ and $pH_{out} = 7.2$ ($pH_{in} = 5.2$). Other conditions as described in Fig. 3. The data are described by Michaelis–Menten kinetics and the solid lines are the result of the fits with nonlinear regression analysis. K_M and v_{max} are the fitting parameters. (B) K_M as a function of pH_{out} (solid squares). Data from Fig. 6A. In addition the fraction of $H_2PO_4^-$ was calculated from Eq. (2) and plotted as a function of pH_{out} (solid circles).

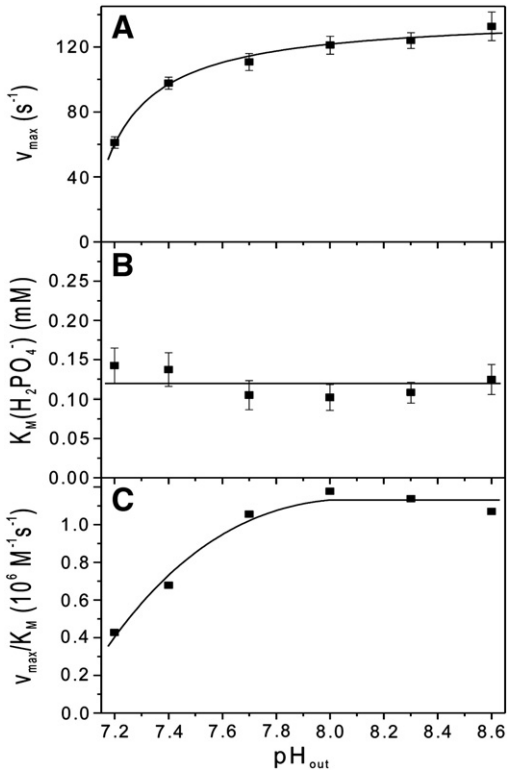

Fig. 7. Analysis of the phosphate dependence of ATP synthesis. (A) Maximal rate of ATP synthesis as function of pH_{out}. Data from Fig. 6A. (B) $K_M(H_2PO_4^-)$ as a function of pH_{out} calculated from K_M and the fraction of the monoanionic species $H_2PO_4^-$ (α). Data from Fig. 6B. (C) Rate constant for binding of $H_2PO_4^-$ $k_1 = \frac{v_{max}}{K_M}$ as function of pH_{out}. Data from Fig. 7A and B.

For an appropriate description of the kinetics, the total P_i concentration in Eq. (1) was substituted by the $H_2PO_4^-$ concentration.

$$\frac{v}{v_{max}} = \frac{[P_i(total)]\alpha}{K_M\alpha + [P_i(total)]\alpha} = \frac{[H_2PO_4^-]}{K_M(H_2PO_4^-) + [H_2PO_4^-]} \quad (3)$$

In this equation $K_M\alpha$ is identical with the K_M for the species $H_2PO_4^-$, i.e. $K_M\alpha = K_M(H_2PO_4)$. The $K_M(H_2PO_4^-)$ has been calculated from the data in Fig. 6B and plotted in Fig. 7B. $K_M(H_2PO_4^-)$ did not depend on pH_{out} and the K_M value for this species is $K_M(H_2PO_4^-) = (120 \pm 20)$ μM.

The $H_2PO_4^-$ concentrations were then calculated from Eq. (2) for all data shown in Fig. 6A and such data were replotted in Fig. 8 as a function of the $H_2PO_4^-$ concentration. The different dependencies on total phosphate concentration shown in Fig. 6A could now be described by a single function with $K_M(H_2PO_4^-) = 120$ μM (continuous line in Fig. 8). From this result we conclude that the substrate of MF_0F_1 in ATP synthesis is the monoanionic species $H_2PO_4^-$.

The rate constant for $H_2PO_4^-$ binding, k_1, can be estimated from the Michaelis–Menten kinetics under the conditions $[S] \ll K_M$ and $k_{cat} \gg k_{-1}$.

$$v = \frac{v_{max}[S]}{K_M + [S]} \approx \frac{v_{max}}{K_M}[S] \approx k_1[S] \quad (4)$$

A plot of $\frac{v_{max}}{K_M}$ as a function of pH_{out} is shown in Fig. 7C. A rate constant of $1.1 \cdot 10^6\ M^{-1}\ s^{-1}$ is obtained at $pH_{out} > 8.0$, below $pH_{out} = 8.0$, the rate constant decreases, since the ΔpH is too low to obtain the maximal rate. This indicates that the minimal rate constant for $H_2PO_4^-$ binding is $k_1 = 1.1 \cdot 10^6\ M^{-1}\ s^{-1}$. Based on this value, the rate constant k_{-1} for P_i dissociation, and the dissociation constant K_D, can be calculated from the definition of K_M and from the value of $k_{cat}\left(k_{cat} = \frac{v_{max}}{[E_0]} = 120\,s^{-1}\right)$, resulting in $k_{-1} = 12\ s^{-1}$ and $K_D = \frac{k_{-1}}{k_1} = 11$ μM, respectively.

4. Discussion

In this work, procedures are described to purify MF_0F_1 from yeast, to reconstitute it into liposomes and to measure high ATP synthesis activities. The turnover number (up to $120\ s^{-1}$) is in the same order of magnitude as that of bovine MF_0F_1 in SMP ($50\ s^{-1}$) and of the

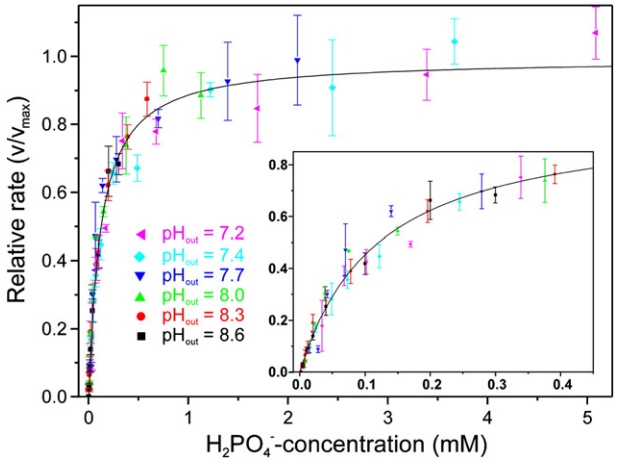

Fig. 8. Rate of ATP synthesis as a function of $H_2PO_4^-$ concentration. The $H_2PO_4^-$ concentrations were calculated from Eq. (2). Inset: $H_2PO_4^-$ concentration below 0.4 mM. Data are from Fig. 6A. The data are described by Michaelis Menten Kinetics. The solid line is obtained by non linear regression analysis ($K_M(H_2PO_4^-) = (120 \pm 20)$ μM, $v_{max} = (120 \pm 20)\ s^{-1}$.

maximal turnover (440 s^{-1}), as estimated in [29], indicating that such isolation and reconstitution procedures largely preserve the native functional state of the enzyme. Since it is assumed that all MF_0F_1 added to the reconstitution mixture is inserted correctly into the liposome membrane and that all MF_0F_1 is active in ATP synthesis, this rate is the minimal turnover of our preparation. Although several isolation and (co-)reconstitution procedures have been reported, this is the first time a rate of ATP synthesis close to the estimated physiological value has been observed for the purified mitochondrial enzyme. Several reasons might be relevant for this high activity.

4.1. Subunit composition

The isolation procedure described here is similar to that reported in [12], and virtually the same band patterns were obtained by SDS-PAGE. Mass spectrometric analysis of the gel revealed that our preparation contained all subunits described previously [49,51–53,59,60] except for the K subunit [49]. Previous reports [12,31,51] had suggested that the subunits e and g dissociate from the complex when using high concentrations of DDM or Triton X-100 for solubilization of monomeric MF_0F_1. Notably, subunits e and g were also found in a preparation of bovine MF_0F_1 that was used for measurement of light-driven ATP synthesis [23]. These subunits have been shown to be involved in dimer/oligomer stabilization and to be not essential for oxidative phosphorylation in vivo [33,59,60]. Our data clearly show that subunit K is not necessary for high activities of the enzyme.

4.2. Monomeric and dimeric MF_0F_1

In recent years, evidence has been accumulating that MF_0F_1 is found in native membranes as dimers and even as oligomers (see [40] and references therein). The dimer-specific subunits (e, g and K) are found at the dimer interface and play a role in dimer stabilization and mitochondrial morphology. A still largely unexplored issue has been whether the monomeric and the multimeric forms are equally competent for catalysis or not. It may be possible that failure to detect high ATP synthesis rates in reconstituted systems was due the fact that the monomeric enzymes were isolated. A higher efficiency of the multimeric forms in vivo has been suggested due to their ability to give rise to inner mitochondrial membrane invaginations, which might be able to sustain a more elevated local protonmotive force [36,37]. As shown by the BN-PAGE analysis of Fig. 1B, the purified enzyme contained only the monomeric form, but it was not possible to exclude that dimerisation took place during the reconstitution procedure, in which the added detergent (Triton X-100) was slowly removed by Biobeads. If more than one enzyme is reconstituted into the same liposome, dimers could be formed. However, the combined measurement of the ATP yield and of the initial rate as a function of the average number of MF_0F_1 per liposome from 0.1 to 10 shows that the high activity is due to the monomeric form or that, if dimerisation does take place, it does not influence the activity (see Fig. 4).

For reconstitution the monomeric MF_0F_1-DDM-micelles and Triton X-100 are added to the liposomes and the detergents are slowly removed. We assume that the interaction between liposome and monomeric MF_0F_1-detergent micelle lead to a Poisson distribution of the number of MF_0F_1 per liposome. However, there is a remote possibility, that at low Triton X-100 concentrations two MF_0F_1-detergent micelles interact in solution and form a dimer before the monomeric MF_0F_1-detergent micelle interacts with the liposome. From statistical reason this is unlikely, however we cannot completely exclude this possibility.

4.3. Reconstitution

For reconstitution of membrane proteins into liposome membranes a number of different procedures have been developed. In our experience two-step procedures with H^+-ATP synthases give higher yields and enzyme activities than one-step procedures [48,54]. In the first step liposomes are formed and in the second step the protein is integrated into the membrane. This allows to use any procedure (dialysis, reverse phase, etc.) for generation of liposomes with an appropriate lipid composition, size distribution etc. without paying special attention to conditions necessary to preserve high enzyme activities. In the second step the liposome membrane is destabilized by addition of an appropriate detergent. The protein-detergent micelles are added and, following their adsorption at the membrane, the protein is integrated. Since it is energetically difficult for the hydrophilic F_1-part to cross the membrane, the insertion is unidirectional, with the large hydrophilic part directed to the outside. Finally, the proteoliposomes with the correctly inserted protein are stabilized by removal of the detergent either by adsorption to BioBeads or by dialysis. After optimisation of the parameters for reconstitution we adopted the procedure described in Materials and methods.

4.4. Reaction conditions for acid–base driven ATP synthesis

The proton motive force ($\Delta\tilde{\mu}_{H^+}$) necessary for ATP synthesis was generated by an acid–base transition and therefore, the initial reaction conditions are well known. In mitochondria, the electric component $\Delta\varphi$ of the protonmotive force is larger than the chemical component ΔpH. To obtain high rates, $\Delta\varphi$ was generated by a large K^+ concentration difference ($[K^+]_{in} = 0.6$ mM, $[K^+]_{out} = 110$ mM in the presence of valinomycin. The permeability coefficient of the K^+/valinomycin complex is large compared to those of the other ions, so that the diffusion potential ($\Delta\varphi = 133$ mV) calculated by the Nernst equation is close to the actual value. An internal K^+ concentration lower than 0.6 mM would not lead to a higher $\Delta\varphi$ since the initial influx of a few K^+ ions compensating the electric membrane capacity would bring the actual internal K^+ concentration to the range of few hundred of μM. Also higher external K^+ concentrations would not increase the actual value of $\Delta\varphi$, since at higher $[K^+]_{in}/[K^+]_{out}$ ratios the membrane is not strictly semipermeable and compensating fluxes of other ions would decrease the diffusion potential.

At $pH_{out} = 8.0$, the rate depended in a sigmoidal way on pH_{in} with a maximal value of 85 s^{-1} reached at $pH_{in} = 5.0$. This dependency reflects the protonation of the enzyme from the inside. Incubation at pH<5.0 might lead to an irreversible denaturation of a fraction of the enzyme and a method is described for correction of this denaturation (see Supplementary Fig. S1). When the constant total phosphate concentration was considered, the dependency of the rate on pH_{out} showed a maximum at $pH_{out} = 7.8$ (Fig. 5A). This indicates the superposition of two opposing effects on the rate. A detailed analysis of the pH_{out} dependency of the Michaelis Menten parameters for phosphate, which took into account the different protonation states of the substrate, was consistent with the hypothesis that the bell-shaped dependency of the rate on pH_{out}, observed in Fig. 5B resulted from the superposition of an increase due to the deprotonation of the enzyme at the outside and of a decrease of the substrate $H_2PO_4^-$ concentration with increasing pH_{out}. After correcting for such decrease, the maximal rate v_{max} reflected only the deprotonation of the enzyme to the outside, and increased correspondingly in a continuous manner, reaching a maximal rate at pH_{out} 8.6 (Fig. 7A).

4.5. Phosphate as substrate in ATP synthesis

The rate of ATP synthesis as a function of the total phosphate concentration can be described by Michaelis–Menten kinetics and both K_M as well as v_{max} depend on pH_{out}. When the concentration of $H_2PO_4^-$ is calculated at different pH_{out} values and the rates are plotted as function of $H_2PO_4^-$ concentration, the phosphate dependencies obtained at different pH_{out} can be described by a single Michaelis–Menten kinetics with $K_M(H_2PO_4^-) = 120$ μM and $v_{max} = 120$ s^{-1} (see

Fig. 8). From these results, we conclude that the substrate for ATP synthesis is the monoanionic species $H_2PO_4^-$.

Earlier results on phosphate binding to F_1 are controversial. Two binding sites with a K_D in the range of 0.1 mM were reported [61]. Under uni-site conditions, a K_D>0.6 mM was calculated for MF_1 [62] and for EF_1, K_D>1 M was obtained [63]. From the increase of K_D with pH it was suggested that $H_2PO_4^-$ was the bound species [63]. Systematic studies of the pH dependency of the K_M values of phosphate have not been carried out yet. K_M-values between 0.2 mM and 1.6 mM for phosphate were observed during ATP synthesis driven by electron transport [64–67], i.e. phosphate binding must occur with high affinity when the enzyme is energized. On the basis of these results, an inhibition of ATP hydrolysis by phosphate is expected, surprisingly, however, no inhibition could be detected during steady state ATP hydrolysis [68,69]. When, however, EF_0F_1 proteoliposomes, which are highly active in ATP synthesis, were used for measurements of the initial rate of proton transport coupled ATP hydrolysis, it was observed that this rate was inhibited by phosphate [70]. The half maximal inhibition occurred at 0.5 mM total phosphate which corresponds to 38 μM $H_2PO_4^-$.

Recent results gave a first approach to understand these contradictions [71]. According to single molecule observations with immobilised TF_1-parts, rotation of the γ-subunit starts with ATP binding (defined as angle 0°) followed by a 80°-step. Phosphate is then released during a 40°-step leading to the final 120°-position. A detailed kinetic analysis of these single molecule data showed that the phosphate affinity differs by orders of magnitude according to when the γ-subunit is at the 80°-position ($K_D(80°) = 4.9$ mM) or at the 120°-position ($K_D(120°) = 70–200$ M). The rate constant for phosphate binding at 80° was $k_1(80°) = 1.7 \cdot 10^5\ M^{-1}\ s^{-1}$.

During proton transport coupled γ-rotation, the direction of rotation is reversed [14], and correspondingly, the step from 120° to 80° increases the phosphate affinity resulting in $K_D = 4.9$ mM. This is close the range required for phosphate binding under physiological conditions. According to the present work, however, from a mechanistic point of view it should be considered that the actual values both for K_M ($K_M(H_2PO_4^-) =$ 120 μM) and for K_D ($K_D(H_2PO_4^-) =$ 11 μM) are still significantly lower. We show here that monoanionic $H_2PO_4^-$ is the species bound. We can use this result to correct the data obtained with total phosphate concentration [71]. At pH 7.0 the fraction of $H_2PO_4^-$ is $\alpha = 0.45$ and therefore, rate constants for $H_2PO_4^-$ binding are increased by a factor 2.2 and the K_D is decreased by a factor 2.2, i.e. the rate constant for binding of $H_2PO_4^-$ is k_1 ($80°, H_2PO_4^-$) $= 3.7 \cdot 10^5\ M^{-1}\ s^{-1}$ (this work $k_1 = 1.1 \cdot 10^6\ M^{-1}\ s^{-1}$) and the dissociation constant is $K_D = 2.2$ mM (this work $K_D = 11$ μM). In addition to this correction it must be considered that the dependency of the affinity on the angle is very steep so that the appropriate K_D relevant for proton transport driven ATP synthesis might be reached at a somewhat lower angle.

Recently, the first crystal structure of yeast F_1 with a phosphate bound in a catalytic site has been reported [72]. A comparison with other high resolution structures of yeast F_1 and bovine F_1 shows that, relative to β_E without phosphate, the γ-subunit is rotated by 16° in the ATP synthesis direction. Presumably, this rotation causes the formation of a phosphate binding site in β_E. This is in accordance with the observation that rotation from 120° and 80° during proton transport driven rotation increases the phosphate affinity into the range necessary for its binding during ATP synthesis [71]. The protonation state cannot be seen in the crystal structure. However, our data show that the phosphate species bound as substrate during ATP synthesis is the monoanionic $H_2PO_4^-$ species.

Supplementary materials related to this article can be found online at doi:10.1016/j.bbabio.2010.07.013.

Acknowledgments

Support from DFG to Wolfgang Haehnel (Ha1084/9) is gratefully acknowledged.

References

[1] A.T. Jagendorf, E. Uribe, ATP formation caused by acid–base transition of spinach chloroplasts, Proc. Natl Acad. Sci. USA 55 (1966) 170–177.
[2] P. Mitchell, Coupling of phosphorylation to electron and hydrogen transfer by a chemi-osmotic type of mechanism, Nature 191 (1961) 144–148.
[3] P. Mitchell, Chemiosmotic coupling in oxidative and photosynthetic phosphorylation, Biol. Rev. Camb. Philos. Soc. 41 (1966) 445–502.
[4] R.A. Capaldi, R. Aggeler, Mechanism of the F(1)F(0)-type ATP synthase, a biological rotary motor, Trends Biochem. Sci. 27 (2002) 154–160.
[5] W. Junge, H. Lill, S. Engelbrecht, ATP synthase: an electrochemical transducer with rotatory mechanics, Trends Biochem. Sci. 22 (1997) 420–423.
[6] K. Kinosita Jr., K. Adachi, H. Itoh, Rotation of F1-ATPase: how an ATP-driven molecular machine may work, Annu. Rev. Biophys. Biomol. Struct. 33 (2004) 245–268.
[7] J. Weber, A.E. Senior, ATP synthase: what we know about ATP hydrolysis and what we do not know about ATP synthesis, Biochim. Biophys. Acta 1458 (2000) 300–309.
[8] M. Yoshida, E. Muneyuki, T. Hisabori, ATP synthase—a marvellous rotary engine of the cell, Nat. Rev. Mol. Cell Biol. 2 (2001) 669–677.
[9] P.D. Boyer, The binding change mechanism for ATP synthase—some probabilities and possibilities, Biochim. Biophys. Acta 1140 (1993) 215–250.
[10] R.L. Cross, The rotary binding change mechanism of ATP synthases, Biochim. Biophys. Acta 1458 (2000) 270–275.
[11] J.P. Abrahams, A.G. Leslie, R. Lutter, J.E. Walker, Structure at 2.8 Å resolution of F_1-ATPase from bovine heart mitochondria, Nature 370 (1994) 621–628.
[12] D. Stock, A.G. Leslie, J.E. Walker, Molecular architecture of the rotary motor in ATP synthase, Science 286 (1999) 1700–1705.
[13] H. Noji, R. Yasuda, M. Yoshida, K. Kinosita Jr., Direct observation of the rotation of F_1-ATPase, Nature 386 (1997) 299–302.
[14] M. Diez, B. Zimmermann, M. Borsch, M. Konig, E. Schweinberger, S. Steigmiller, R. Reuter, S. Felekyan, V. Kudryavtsev, C.A. Seidel, P. Gräber, Proton-powered subunit rotation in single membrane-bound F_0F_1-ATP synthase, Nat. Struct. Mol. Biol. 11 (2004) 135–141.
[15] B. Zimmermann, M. Diez, N. Zarrabi, P. Gräber, M. Borsch, Movements of the epsilon-subunit during catalysis and activation in single membrane-bound H(+)-ATP synthase, EMBO J. 24 (2005) 2053–2063.
[16] M. Bokranz, E. Morschel, A. Kroger, Phosphorylation and phosphate-ATP exchange catalyzed by the ATP synthase isolated from Wolinella succinogenes, Biochim. Biophys. Acta 810 (1985) 332–339.
[17] S. Fischer, C. Etzold, P. Turina, G. Deckers-Hebestreit, K. Altendorf, P. Graber, ATP synthesis catalyzed by the ATP synthase of Escherichia coli reconstituted into liposomes, Eur. J. Biochem. 225 (1994) 167–172.
[18] G. Schmidt, P. Gräber, The rate of ATP synthesis by reconstituted CF0F1 liposomes, Biochim. Biophys. Acta 808 (1985) 46–51.
[19] L. Slooten, S. Vandenbranden, ATP-synthesis by proteoliposomes incorporating Rhodospirillum rubrum F0F1 as measured with firefly luciferase: dependence on delta psi and delta pH, Biochim. Biophys. Acta 976 (1989) 150–160.
[20] N. Sone, M. Yoshida, H. Hirata, Y. Kagawa, Reconstitution of vesicles capable of energy transformation from phospholipids and adenosine triphosphatase of a thermophilic bacterium, J. Biol. Chem. 252 (1977) 2956–2960.
[21] H.S. van Walraven, R.L. van der Bend, M.J.M. Hagendoorn, N.P. Haak, A. Oskam, A. Oostdam, K. Krab, R. Kraayenhof, Comparison of ATP synthesis efficiencies in ATPase proteoliposomes of different complexities, Bioelectrochem. Bioenerg. 16 (1986) 167–180.
[22] W.S. Thayer, P.C. Hinkle, Synthesis of adenosine triphosphate by an artificially imposed electrochemical proton gradient in bovine heart submitochondrial particles, J. Biol. Chem. 250 (1975) 5330–5335.
[23] G. Groth, J.E. Walker, ATP synthase from bovine heart mitochondria: reconstitution into unilamellar phospholipid vesicles of the pure enzyme in a functional state, Biochem. J. 318 (Pt 1) (1996) 351–357.
[24] B. Lang, G. Burger, I. Doxiadis, D.Y. Thomas, W. Bandlow, F. Kaudewitz, A simple method for the large-scale preparation of mitochondria from microorganisms, Anal. Biochem. 77 (1977) 110–121.
[25] R. Lutter, M. Saraste, H.S. van Walraven, M.J. Runswick, M. Finel, J.F. Deatherage, J.E. Walker, F1F0-ATP synthase from bovine heart mitochondria: development of the purification of a monodisperse oligomycin-sensitive ATPase, Biochem. J. 295 (Pt 3) (1993) 799–806.
[26] E. Vazquez-Contreras, M.T. de Gomez-Puyou, G. Dreyfus, A column centrifugation method for the reconstitution in liposomes of the mitochondrial F0F1 ATP synthase/ATPase, Protein Expr. Purif. 7 (1996) 55–59.
[27] S. Matuschka, K. Zwicker, T. Nawroth, G. Zimmer, ATP synthesis by purified ATP-synthase from beef heart mitochondria after coreconstitution with bacteriorhodopsin, Arch. Biochem. Biophys. 322 (1995) 135–142.
[28] B. Pitard, P. Richard, M. Dunach, J.L. Rigaud, ATP synthesis by the F0F1 ATP synthase from thermophilic Bacillus PS3 reconstituted into liposomes with bacteriorhodopsin. 2. Relationships between proton motive force and ATP synthesis, Eur. J. Biochem. 235 (1996) 779–788.
[29] A. Matsuno-Yagi, Y. Hatefi, Estimation of the turnover number of bovine heart F0F1 complexes for ATP synthesis, Biochemistry 27 (1988) 335–340.
[30] P. Richard, B. Pitard, J.L. Rigaud, ATP synthesis by the F0F1-ATPase from the thermophilic Bacillus PS3 co-reconstituted with bacteriorhodopsin into liposomes. Evidence for stimulation of ATP synthesis by ATP bound to a noncatalytic binding site, J. Biol. Chem. 270 (1995) 21571–21578.
[31] I. Arnold, K. Pfeiffer, W. Neupert, R.A. Stuart, H. Schagger, Yeast mitochondrial F_1F_0-ATP synthase exists as a dimer: identification of three dimer-specific subunits, EMBO J. 17 (1998) 7170–7178.

[32] G. Arselin, M.F. Giraud, A. Dautant, J. Vaillier, D. Brethes, B. Coulary-Salin, J. Schaeffer, J. Velours, The GxxxG motif of the transmembrane domain of subunit e is involved in the dimerization/oligomerization of the yeast ATP synthase complex in the mitochondrial membrane, Eur. J. Biochem. 270 (2003) 1875–1884.
[33] V. Soubannier, J. Vaillier, P. Paumard, B. Coulary, J. Schaeffer, J. Velours, In the absence of the first membrane-spanning segment of subunit 4(b), the yeast ATP synthase is functional but does not dimerize or oligomerize, J. Biol. Chem. 277 (2002) 10739–10745.
[34] N. Buzhynskyy, P. Sens, V. Prima, J.N. Sturgis, S. Scheuring, Rows of ATP synthase dimers in native mitochondrial inner membranes, Biophys. J. 93 (2007) 2870–2876.
[35] N.V. Dudkina, J. Heinemeyer, W. Keegstra, E.J. Boekema, H.P. Braun, Structure of dimeric ATP synthase from mitochondria: an angular association of monomers induces the strong curvature of the inner membrane, FEBS Lett. 579 (2005) 5769–5772.
[36] M. Strauss, G. Hofhaus, R.R. Schroder, W. Kuhlbrandt, Dimer ribbons of ATP synthase shape the inner mitochondrial membrane, EMBO J. 27 (2008) 1154–1160.
[37] C. Bornhovd, F. Vogel, W. Neupert, A.S. Reichert, Mitochondrial membrane potential is dependent on the oligomeric state of F1F0-ATP synthase supracomplexes, J. Biol. Chem. 281 (2006) 13990–13998.
[38] M. Prescott, N.C. Bush, P. Nagley, R.J. Devenish, Properties of yeast cells depleted of the OSCP subunit of mitochondrial ATP synthase by regulated expression of the ATP5 gene, Biochem. Mol. Biol. Int. 34 (1994) 789–799.
[39] S.C. Gill, P.H. von Hippel, Calculation of protein extinction coefficients from amino acid sequence data, Anal. Biochem. 182 (1989) 319–326.
[40] R.J. Devenish, M. Prescott, A.J. Rodgers, The structure and function of mitochondrial F1F0-ATP synthases, Int. Rev. Cell Mol. Biol. 267 (2008) 1–58.
[41] H. Schagger, G. von Jagow, Tricine-sodium dodecyl sulfate-polyacrylamide gel electrophoresis for the separation of proteins in the range from 1 to 100 kDa, Anal. Biochem. 166 (1987) 368–379.
[42] P. Schopfer, E. Heyno, F. Drepper, A. Krieger-Liszkay, Naphthoquinone-dependent generation of superoxide radicals by quinone reductase isolated from the plasma membrane of soybean, Plant Physiol. 147 (2008) 864–878.
[43] L.Y. Geer, S.P. Markey, J.A. Kowalak, L. Wagner, M. Xu, D.M. Maynard, X. Yang, W. Shi, S.H. Bryant, Open mass spectrometry search algorithm, J. Proteome Res. 3 (2004) 958–964.
[44] H. Heide, A. Nordhues, F. Drepper, S. Nick, M. Schulz-Raffelt, W. Haehnel, M. Schroda, Application of quantitative immunoprecipitation combined with knockdown and cross-linking to Chlamydomonas reveals the presence of vesicle-inducing protein in plastids 1 in a common complex with chloroplast HSP90C, Proteomics 9 (2009) 1–12.
[45] W.X. Schulze, M. Mann, A novel proteomic screen for peptide–protein interactions, J. Biol. Chem. 279 (2004) 10756–10764.
[46] M. Andresen, M.C. Wahl, A.C. Stiel, F. Grater, L.V. Schafer, S. Trowitzsch, G. Weber, C. Eggeling, H. Grubmuller, S.W. Hell, S. Jakobs, Structure and mechanism of the reversible photoswitch of a fluorescent protein, Proc. Natl. Acad. Sci. U. S. A. 102 (2005) 13070–13074 Epub 12005 Aug 13031.
[47] S. Fischer, P. Gräber, Comparison of Delta pH- and Delta phi-driven ATP synthesis catalyzed by the H^+-ATPases from Escherichia coli or chloroplasts reconstituted into liposomes, FEBS Lett. 457 (1999) 327–332.
[48] J.L. Rigaud, M.T. Paternostre, A. Bluzat, Mechanisms of membrane protein insertion into liposomes during reconstitution procedures involving the use of detergents. 2. Incorporation of the light-driven proton pump bacteriorhodopsin, Biochemistry 27 (1988) 2677–2688.
[49] I. Wittig, J. Velours, R. Stuart, H. Schagger, Characterization of domain interfaces in monomeric and dimeric ATP synthase, Mol. Cell. Proteomics 7 (2008) 995–1004.
[50] J. Velours, G. Arselin, The Saccharomyces cerevisiae ATP synthase, J. Bioenerg. Biomembr. 32 (2000) 383–390.
[51] G. Arselin, J. Vaillier, P.V. Graves, J. Velours, ATP synthase of yeast mitochondria. Isolation of the subunit h and disruption of the ATP14 gene, J. Biol. Chem. 271 (1996) 20284–20290.
[52] R.J. Devenish, M. Prescott, X. Roucou, P. Nagley, Insights into ATP synthase assembly and function through the molecular genetic manipulation of subunits of the yeast mitochondrial enzyme complex, Biochim. Biophys. Acta 1458 (2000) 428–442.
[53] Y.H. Ko, J. Hullihen, S. Hong, P.L. Pedersen, Mitochondrial F(0)F(1) ATP synthase. Subunit regions on the F1 motor shielded by F(0), Functional significance, and evidence for an involvement of the unique F(0) subunit F(6), J. Biol. Chem. 275 (2000) 32931–32939.
[54] P. Richard, J.L. Rigaud, P. Graber, Reconstitution of CF0F1 into liposomes using a new reconstitution procedure, Eur. J. Biochem. 193 (1990) 921–925.
[55] H. Ruf, Y. Georgalis, E. Grell, Dynamic laser light scattering to determine size distributions of vesicles, Meth. Enzymol. 172 (1989) 364–390.
[56] J.F. Nagle, R. Zhang, S. Tristram-Nagle, W. Sun, H.I. Petrache, R.M. Suter, X-ray structure determination of fully hydrated L alpha phase dipalmitoylphosphatidylcholine bilayers, Biophys. J. 70 (1996) 1419–1431.
[57] F.E. Possmayer, P. Gräber, The pH_{in} and pH_{out} dependence of the rate of ATP synthesis catalyzed by the chloroplast H^+-ATPase, CF_0F_1, in proteoliposomes, J. Biol. Chem. 269 (1994) 1896–1904.
[58] K. Krab, J. van Wezel, Improved derivation of phosphate potentials at different temperatures, Biochim. Biophys. Acta 1098 (1992) 172–176.
[59] G.M. Boyle, X. Roucou, P. Nagley, R.J. Devenish, M. Prescott, Identification of subunit g of yeast mitochondrial F1F0-ATP synthase, a protein required for maximal activity of cytochrome c oxidase, Eur. J. Biochem. 262 (1999) 315–323.
[60] P. Paumard, J. Vaillier, B. Coulary, J. Schaeffer, V. Soubannier, D.M. Mueller, D. Brethes, J.P. di Rago, J. Velours, The ATP synthase is involved in generating mitochondrial cristae morphology, EMBO J. 21 (2002) 221–230.
[61] H.S. Penefsky, Pi binding by the F1-ATPase of beef heart mitochondria and of the Escherichia coli plasma membrane, FEBS Lett. 579 (2005) 2250–2252.
[62] C. Grubmeyer, R.L. Cross, H.S. Penefsky, Mechanism of ATP hydrolysis by beef heart mitochondrial ATPase. Rate constants for elementary steps in catalysis at a single site, J. Biol. Chem. 257 (1982) 12092–12100.
[63] M.K. al-Shawi, A.E. Senior, Catalytic sites of Escherichia coli F1-ATPase. Characterization of unisite catalysis at varied pH, Biochemistry 31 (1992) 878–885.
[64] M.K. Al-Shawi, C.J. Ketchum, R.K. Nakamoto, The Escherichia coli FOF1 gammaM23K uncoupling mutant has a higher K0.5 for Pi. Transition state analysis of this mutant and others reveals that synthesis and hydrolysis utilize the same kinetic pathway, Biochemistry 36 (1997) 12961–12969.
[65] Y. Hatefi, T. Yagi, D.C. Phelps, S.Y. Wong, S.B. Vik, Y.M. Galante, Substrate binding affinity changes in mitochondrial energy-linked reactions, Proc. Natl Acad. Sci. USA 79 (1982) 1756–1760.
[66] C. Kayalar, J. Rosing, P.D. Boyer, 2, 4-Dinitrophenol causes a marked increase in the apparent Km of Pi and of ADP for oxidative phosphorylation, Biochem. Biophys. Res. Commun. 72 (1976) 1153–1159.
[67] S.M. Schuster, G.D. Reinhart, H.A. Lardy, Studies on the kinetic mechanism of oxidative phosphorylation, J. Biol. Chem. 252 (1977) 427–432.
[68] A.D. Vinogradov, Steady-state and pre-steady-state kinetics of the mitochondrial F(1)F(o) ATPase: is ATP synthase a reversible molecular machine? J. Exp. Biol. 203 (2000) 41–49.
[69] T.V. Zharova, A.D. Vinogradov, Energy-linked binding of Pi is required for continuous steady-state proton-translocating ATP hydrolysis catalyzed by F0.F1 ATP synthase, Biochemistry 45 (2006) 14552–14558.
[70] S. Fischer, P. Gräber, P. Turina, The activity of the ATP synthase from Escherichia coli is regulated by the transmembrane proton motive force, J. Biol. Chem. 275 (2000) 30157–30162.
[71] K. Adachi, K. Oiwa, T. Nishizaka, S. Furuike, H. Noji, H. Itoh, M. Yoshida, K. Kinosita Jr., Coupling of rotation and catalysis in F(1)-ATPase revealed by single-molecule imaging and manipulation, Cell 130 (2007) 309–321.
[72] V. Kabaleeswaran, N. Puri, J.E. Walker, A.G. Leslie, D.M. Mueller, Novel features of the rotary catalytic mechanism revealed in the structure of yeast F1 ATPase, EMBO J. 25 (2006) 5433–5442.